Q-carbon as an emergent surface coating material for antimicrobial applications

Naveen Joshi[1], Shubhangi Shukla[2], Nayna Khosla[1], Lyndsi Vanderwal[3], Shane Stafslien[3], Jagdish Narayan[1], and Roger J. Narayan[1]*

1. Department of Materials Science and Engineering, Centennial Campus, North Carolina State University, Raleigh, NC, 27695-7907, USA
2. Joint Department of Biomedical Engineering, Centennial Campus, North Carolina State University, Raleigh, NC, 27695-7115, USA
3. Department of Coatings and Polymeric Materials, North Dakota State University, Fargo, ND, USA

Abstract:

Q-carbon, an allotrope of carbon, exhibits exciting functional properties and robust mechanical strength. We propose that the surface of the Q-carbon can be functionalized by doping it with silicon to enhance its performance as a potential implant material. As such, a coating of silicon-doped Q-carbon (Si-Q-carbon) is shown to minimize the formation of biofilm, thus reducing the risk of microbial infection. We report the formation of Si-Q-carbon coatings of varied thicknesses (10 nm and 20 nm) through the plasma-enhanced chemical vapor deposition technique. The surface composition and the bonding characteristics of the thin films were evaluated by Raman spectroscopy, XPS, and EELS studies, which showed that the thinnest sample (10 nm) has a high sp^3 content of ~85%. Furthermore, wettability and surface energy calculations were undertaken to investigate the surface characteristics of the coatings. The 10 nm sample was found to be more hydrophilic with a water contact angle of 75.3° (± 0.6°). The antibacterial activity of Si-Q-carbon coatings was investigated using a *Staphylococcus epidermidis* agar plating technique, and the adhesion of bacteria was explained in terms of the surface properties of the thin films. We demonstrate that the Si-Q-carbon coating with the highest sp^3 content is hydrophilic and showed a 57% reduction in adhered biofilm relative to a glass control. We envisage the potential application of Q-carbon in arthroplasty devices with enhanced mechanical strength and resistance to periprosthetic joint infections.

Keywords: adhesion; antibacterial coatings; hydrophilicity; Q-carbon; surface properties.

1. Introduction

Carbon-based materials have gained much attention in biomedical research due to their exceptional biocompatibility, chemical stability, and outstanding mechanical properties [1]. Among them, diamond-like carbon (DLC) is widely explored as a potential medical implant material due to its enhanced resistance to corrosion [2], anti-inflammatory properties [3], antimicrobial activity [4], and improved tribological properties [5]. Furthermore, DLC coatings can be grown on various substrates at relatively low deposition temperatures [6], making this class of carbon-based materials economically and technologically important.

A number of thin film deposition techniques have been reported for the growth of DLC coatings, including chemical vapor deposition (CVD) and physical vapor deposition (PVD) techniques [7]. Popular PVD techniques include pulsed laser deposition [8], plasma source ion implantation [9], and magnetron sputtering [10]. Attempts were made to develop DLC coatings with improved mechanical strength and corrosion resistance for applications in the aerospace industry. Due to the versatile functionality of DLC coatings, special emphasis was placed on developing coatings that are bio- and hemocompatible. The CVD techniques were widely explored to grow biocompatible DLC coatings as they enabled the deposition of coatings with conformal coverage. Furthermore, CVD techniques produced uniform film over a large area [11]. The plasma-enhanced CVD (PECVD) technique enhanced sp^3 content; it is widely utilized for the deposition of conformal DLC coatings due to its suitability for large-scale manufacturing [12] and ease of synthesis [13]. Unlike the conventional CVD technique, in which precursor gases are allowed to react immediately with the preheated substrates to grow films, PECVD employs the generation of plasma to provide energy for the deposition reactions to occur at lower substrate temperatures. As such, films grown through PECVD are strain-free and adherent [14]. Moreover, Gotzmann et al. have shown that PECVD-grown DLC coatings are biocompatible [15]. Silicon is incorporated into DLC to improve the thermal stability [16], enhance the adhesion of the coating to the underlying substrate, and reduce the internal stresses in the film [17]. Liu et al. have demonstrated that the addition of Si to DLC implant devices has reduced the generation of an inflammatory reaction [18]. Furthermore, Si prefers to form sp^3 bonding states within covalent compounds and is known to increase the sp^3/sp^2 ratio in DLC films [19]. An sp^3-rich layer reduces the adhesion of bacteria to the surface, enhancing the potential inhibition of microorganisms [20]. In addition, Yang et al. have shown that Si-incorporated DLC coatings exhibit promising antifungal properties, making them suitable candidates for use in medical implants [21].

However, silicon-incorporated DLC (Si-DLC) shows many strain-localized regions under tensile loading, lowering the stress-bearing capacity of the film [22]. It is also demonstrated that an increase in temperature decreases the ultimate tensile strength of Si-DLC [23], potentially limiting the lifespan of medical implants. Thus, even though Si-DLC coatings have shown promising characteristics for use in a medical implant, they require regular replacement as they degrade over time. Moreover, replacement procedures lead to an increased cost of operation and expose the subject to the threat of infection. This situation demands an implant material that is mechanically robust, adherent to the substrate, chemically inert, and biocompatible.

Quenched-in carbon or Q-carbon is an allotrope of carbon with extraordinary structural and mechanical properties [24]. Q-carbon contains randomly packed tetrahedra with a high sp^3/sp^2 ratio at its interface [24-25]. It is known to be harder than diamond because it contains a higher number density of covalently-bonded carbon atoms [24, 26]. Thus Q-carbon may serve as an ideal ultrahard coating as it is more adherent, harder, and tougher than diamond [24-26]. Recently, our group demonstrated the large-scale synthesis of Si-incorporated Q-carbon (Si-Q-carbon) thin films by the low-energy ion bombardment PECVD technique and showed that Si-Q-carbon is chemically analogous to Si-DLC with tunable sp^3-content [27]. However, the suitability of Q-carbon for biomedical applications has yet to be established.

In the present work, we report on the formation of sp^3-rich Si-doped Q-carbon thin films on glass substrates via the PECVD technique and show that Si-Q-carbon can be an excellent replacement for Si-DLC coatings for medical implant applications. As-deposited Si-Q-carbon films were investigated for their antibacterial activity. The study was conducted to evaluate *in vitro* the adhesion capability of a model microorganism, *Staphylococcus epidermidis* (*S. epidermidis*), to the Si-Q-carbon surface and to correlate these findings with surface properties. The surface composition and bonding characteristics, including the sp^3/sp^2 content, were investigated via XPS, Raman spectroscopy, and EEL spectroscopy. The wettability and hydrophilic character of the films were investigated using water contact angle measurements. As such, the potential of Si-Q-carbon layers as a potential antimicrobial coating was considered via an estimation of the interfacial energy between the Si-Q-carbon surface and several test liquids. *S. epidermidis* is a bacterial species that is commonly identified for causing infection in medical devices due to its ability to attach to implant surfaces and form biofilms [28]. Biofilms are associated with enhanced resistance to antimicrobial agents, leading to chronic infections. The lifecycle of *S. epidermidis* biofilm is classified into three stages: (i) initial adhesion of the biofilm, (ii) biofilm accumulation followed by biofilm maturation, and

(iii) biofilm disassembly [28-29]. In the first stage, bacteria begin to grow and adhere to the surface; bacteria form a biofilm in the second stage. In the last stage, the biofilm disassembles to release the bacterial cells to react with the host immune system. This situation necessitates the development of biomedical device coatings that are inherently capable of preventing the adhesion of bacteria and the formation of a biofilm as early as its second stage. Thus, *S. epidermidis* was chosen to evaluate bacterial adhesion on Si-Q-carbon films. Through this study, we demonstrate that Q-carbon holds great promise for preventing bacterial infections due to its superior functional properties as compared to DLC coatings [30].

2. Materials and Methods

2.1 Deposition of Si-incorporated Q-carbon (Si-Q-carbon) thin films

Si-Q-carbon thin films were deposited using the Radio Frequency Plasma-Enhanced Chemical Vapor Deposition technique as described by Riley et al. [27]. Microscopy glass slides of dimensions 15 mm X 15 mm were used as substrates for the deposition of Si-Q-Carbon thin films. Substrates were cleaned through ultrasonication in an acetone bath for 5 min, followed by the methanol bath for another 5 min; they were immediately transferred to the chamber for deposition. The PECVD system is a custom-designed instrument that generates plasma via the capacitively coupled mode. A schematic of the PECVD system utilized for the deposition of Si-Q-carbon is shown in Figure 1. The pumping system provides a base pressure of approximately 2.67 x 10^{-6} Pa. The process gases flow from above inside the chamber and via a showerhead distribution ring apparatus. The deposition process involves loading, plasma cleaning, plasma deposition, post-processing, and unloading steps. After an overnight pump-down step to reach a base pressure of 1.33 x 10^{-6} Pa, the plasma cleaning procedure was undertaken for 10 min with argon gas; a mass flow rate of 90 SCCM was used in this study. The deposition was performed using 1.6 SCCM of trimethylsilane and 90 SCCM of argon over 3 min and 4.5 min to obtain the 10 nm and 20 nm samples, respectively. The deposition process involved a peak-to-peak voltage (V_{pp}) of 300 ±10V, a DC bias of -150 ± 10 V, and an RF power of 83 ± 10 W. The post-processing plasma treatment involved exposure to 90 SCCM argon gas for 5 min; a V_{pp} of 500 ± 10 V, an RF power of 160 ± 10 W, and a DC bias of 250 ± 10 V were used in this study. During these procedures, the total pressure was kept at 6.67 Pa per a MKS Baratron gauge (Andover, MA, USA).

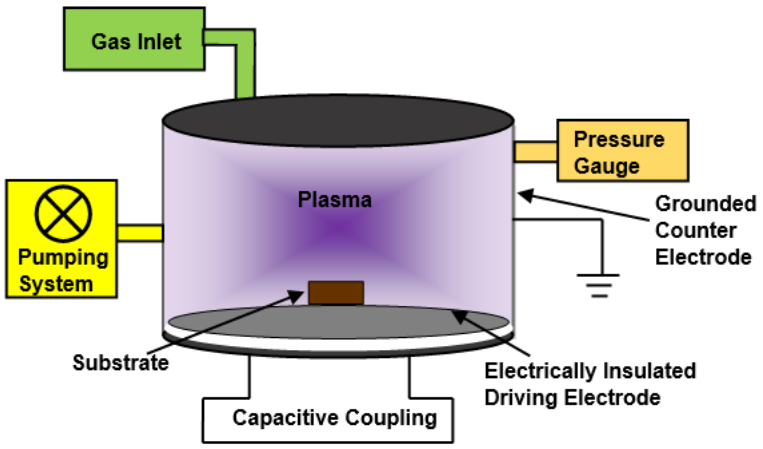

Figure 1. *Schematic of the PECVD chamber utilized for the deposition of Si-Q-carbon thin films.*

2.1 Surface characterization

The thickness of the samples (10 nm and 20 nm) was estimated using the contact profilometry method via the step-height measurement approach using a Veeco Dektak D150 instrument (Model: Dektak 150; Plainview, New York, USA); a tip size of 12.5 µm in radius was used in this study. The surface roughness of the Si-Q-carbon coating was assessed via atomic force microscopy (AFM) using an MFP-3D-BIO AFM (Oxford Instruments Asylum Research, Santa Barbara, CA, USA); the surface roughness of the deposited films was evaluated using this approach. The AFM images containing 5 µm x 5 µm scans were acquired under ambient conditions using tapping mode with a 300 kHz resonant frequency.

2.2 Surface composition and structural characterization

Raman spectroscopy was employed to investigate the bonding characteristics and sp^3 content in Si-Q-carbon films. Measurements were done using an alpha300M WITec confocal microscope system (Ulm, Germany) equipped with a 532 nm solid-state laser as well as a UHTS 300 spectrometer. The grating size is 600 l/mm, and the spot size of the laser is ~ 2 µm in diameter. The Raman signals were calibrated with the characteristic peak of Si (520.6 cm^{-1}). X-ray photoelectron Spectroscopy (XPS) was utilized to understand the surface composition of the thin films. Measurements were undertaken on a Kratos XPS system (Shimadzu Corporation, Kyoto, Japan) with an X-ray excitation source of monochromated aluminum K_α radiation (λ=1.487 keV). A pass energy of 160 eV and 20 eV were used for the survey scan and the region scan, respectively. All the data were calibrated to the C-C peak at 284.8 eV. The Shirley model was utilized for the background omission; the Gaussian distribution model was utilized to establish the deconvoluted peaks. Peak intensity

fitting was performed considering the FWHM of the individual peaks using the OriginPro software. The cross-sectional images, the energy-dispersive X-ray analysis data, and electron energy-loss spectroscopy (EELS) were performed using a high-resolution transmission electron microscope (S/TEM, Talos-F200 microscope, Hillsboro, OR, USA). The EELS data were obtained with a collection semi-angle of 5 mrad and a dispersion of 0.25 eV/channel. Samples for TEM analysis were created using a focused ion beam (FIB) technique (Quanta 3D FEG, FEI, Hillsboro, OR, USA).

2.3 Wettability and Surface Energy

The surface energy of the Si-Q-carbon thin films was determined by wettability measurements, which were carried out by using deionized water as a test liquid. The Owens-Wendt model was used to estimate the surface energy components of the sample [31]. According to the Owens-Wendt model, the dispersive component of the surface energy is associated with van der Waals forces and other non-site specific interactions, and the polar component is associated with hydrogen bonding and dipole-dipole interactions [31]. Young's equation describes the wetting of a solid surface by a liquid; it is given as follows:

$$\gamma_S - \gamma_{SL} = \gamma_L \cos\vartheta \qquad (1)$$

In this equation, γ_S, γ_L, and γ_{SL} are free energies of the solid, liquid, and solid-liquid interface, respectively. The contact angle between the liquid and the solid surface is designated θ. The surface and interfacial free energy components can be resolved into their dispersive (d) and polar (p) components:

$$\gamma_S = \gamma_S^d + \gamma_S^p \qquad (2a)$$

$$\gamma_L = \gamma_L^d + \gamma_L^p \qquad (2b)$$

$$\gamma_{SL} = \gamma_{SL}^d + \gamma_{SL}^p \qquad (2c)$$

By expressing (1) as

$$(1+\cos\vartheta)\,\gamma_L = \gamma_S + \gamma_L - \gamma_{SL} \qquad (3)$$

And substituting (2) in (3), we get

$$(1+\cos\vartheta)\,\gamma_L = (\gamma_S^d + \gamma_L^d - \gamma_{SL}^d) + (\gamma_S^p + \gamma_L^p - \gamma_{SL}^p) \qquad (4)$$

The dispersive component associated with the interfacial tension between the solid and the liquid is provided by the Good-Girifalco-Fowkes rule [32]:

$$\gamma_{SL}^d = \gamma_S^d + \gamma_L^d - 2\,(\gamma_S^d \gamma_L^d)^{0.5} \qquad (5a)$$

The polar component is expressed as shown by van Oss et al.

$$\gamma_{SL}^{p} = \gamma_{S}^{p} + \gamma_{L}^{p} - 2\,(\gamma_{S}^{p}\,\gamma_{L}^{p})^{0.5} \qquad (5b)$$

By substituting the equations (5a) and (5b) in (4), Young's equation can be rewritten as

$$\gamma_{L}[(1+\cos\vartheta)/2] = (\gamma_{S}^{d}\,\gamma_{L}^{d})^{0.5} + (\gamma_{S}^{p}\,\gamma_{L}^{p})^{0.5} \qquad (6)$$

The dispersive and polar components of the solid surface energy can be determined by assessing the contact angle of different liquids with known values of γ_{L}^{d} and γ_{L}^{p} [33]. The water contact angle of the Si-Q-carbon films (10 nm and 20 nm) was measured by the OCA 200 contact angle goniometer and drop shape analysis instrument (DataPhysics Instruments USA Corp., Charlotte, NC, USA). An average of ten measurements were acquired to calculate the contact angle value.

2.4 Antibacterial Activity

Assessments of the antibacterial activity of the Si-Q-carbon materials were performed utilizing a method described by Pezzotti et al. [34]. Briefly, a cryopreserved stock of *S. epidermidis* was plated onto tryptic soy agar (TSA) and then incubated at 37 °C for 24 hours; a single colony was subsequently transferred to tryptic soy broth (TSB) and cultured overnight at 37 °C. A 100 µl aliquot of the overnight bacterial suspension in TSB was spread onto individual TSA agar plates. Three replicates of Si-Q-carbon-coated and uncoated glass samples were then placed in contact with the inoculated agar; incubation of the agar was performed at 37 °C under aerobic conditions for 24 hours. Bacterial colonization and viability on the Si-Q carbon and control samples were observed by epifluorescence microscopy (Olympus, Breinigsville, PA). To facilitate visualization, bacteria were stained using two different solutions: (i) 4',6-diamidino-2-phenylindole (DAPI), which stains bacterial DNA a blue color, and ii) Sytox Green nucleic acid dye, which stains dead bacteria only with a green color. Images were taken at 20X magnification with DAPI and FITC filters.

3. Results and Discussions

AFM measurements were performed to understand the changes in surface roughness and its consequence on the antibacterial properties in the as-deposited Si-Q-carbon samples. Roughness is known to influence the growth kinetics, density, and texture of a biofilm [35]. Surface roughness leads to the primary adhesion of bacteria and is found to be effective in shielding the biofilm from being detached. Thus, higher roughness contributes to bacterial immobilization, resulting in a high rate of biofilm formation [35-36]. The 2D roughness scans and the corresponding depth versus distance profilesof the samples are shown in Figure 2. The root-mean-square (rms) values obtained from AFM measurements were

found to be 183.234 pm (std. deviation = 183.236 pm) and 769.294 pm (std. deviation = 769.299 pm) for the 10 nm and 20 nm samples, respectively. These results suggest that Si doping enhances the proportion of sigma bonds, leading to a higher rms value in the thicker sample [37]. Furthermore, the change in roughness in the samples is attributed to the etching of carbon atoms since the phenomenon is known to increase with increasing film thickness. Thus Si-Q-carbon samples show antibacterial properties without the inclusion of additional antimicrobial agents. These results are consistent with the contact angle measurements and bacterial adhesion data described in the subsequent sections.

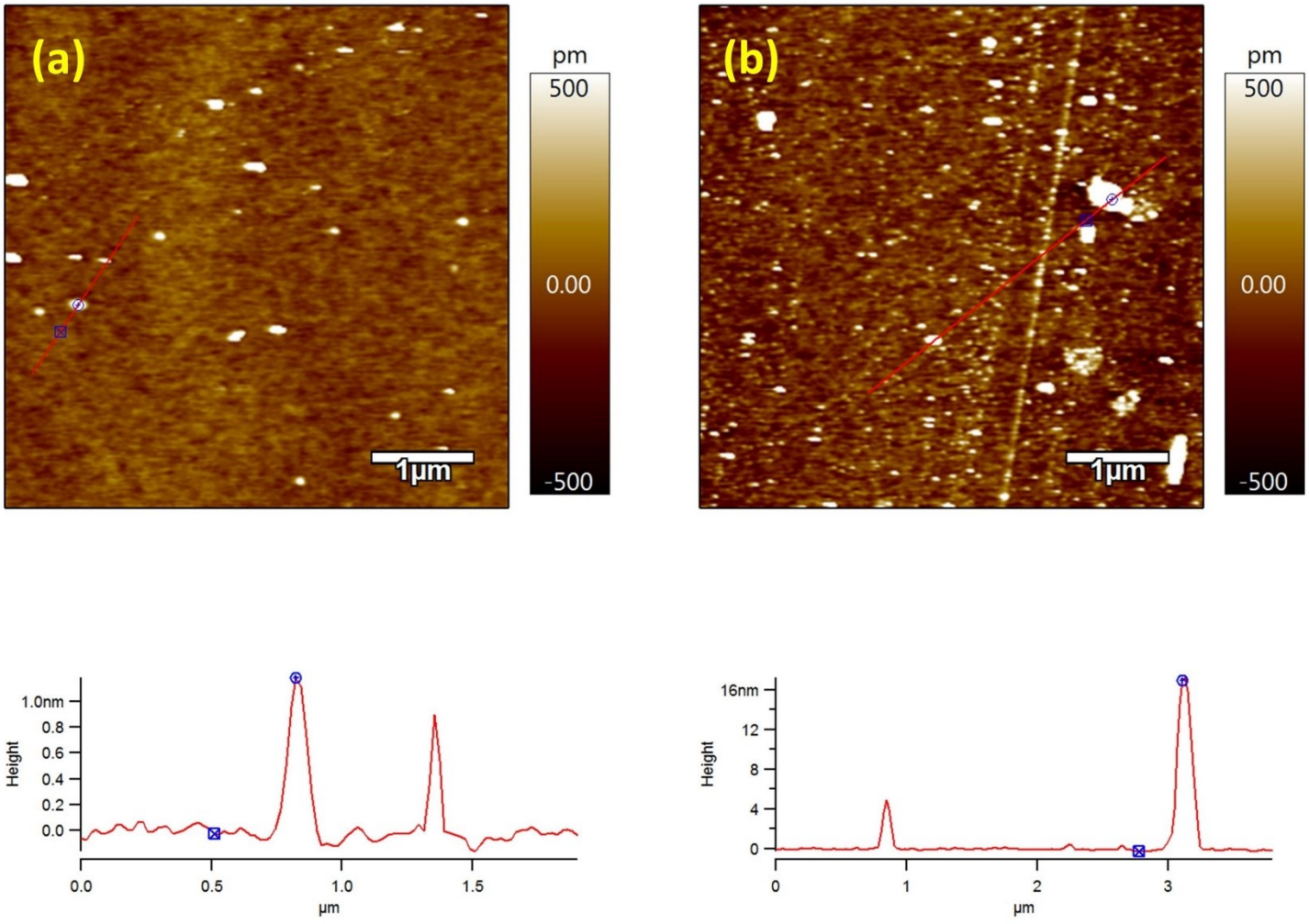

Figure 2. *2D surface roughness scans and the corresponding depth profiles of Si-Q-carbon samples with a thickness of: (a) 10 nm (b) 20 nm.*

Raman spectral analysis was performed to understand the molecular vibrational modes and bonding in the sample (Figure 3). Gaussian fitting was employed to deconvolute the peaks; all the samples could be deconvoluted into two peaks. The peak at 1320 cm^{-1} (D peak) was assigned to the breathing mode of the sp^2 bonds, which is associated with the presence of defects in the structure [38]. The second fitted peak at 1485 cm^{-1}, which is referred to as the G peak, is associated with the stretching of the sp^2-bonds in rings or chains [39]. Since Si can only form fourfold-coordinated links with carbon atoms, the sp^3 content in the Si-doped structures increases [27]. The I_D/I_G values for the Si-Q-carbon thin films of 10 nm and 20 nm thicknesses were found to be 0.15 and 0.27, respectively; the higher sp^3/sp^2 value was associated with the thinner sample. These results reveal an enhancement in the sp^3 content of Si-Q-carbon as compared to Si-DLC structures [40].

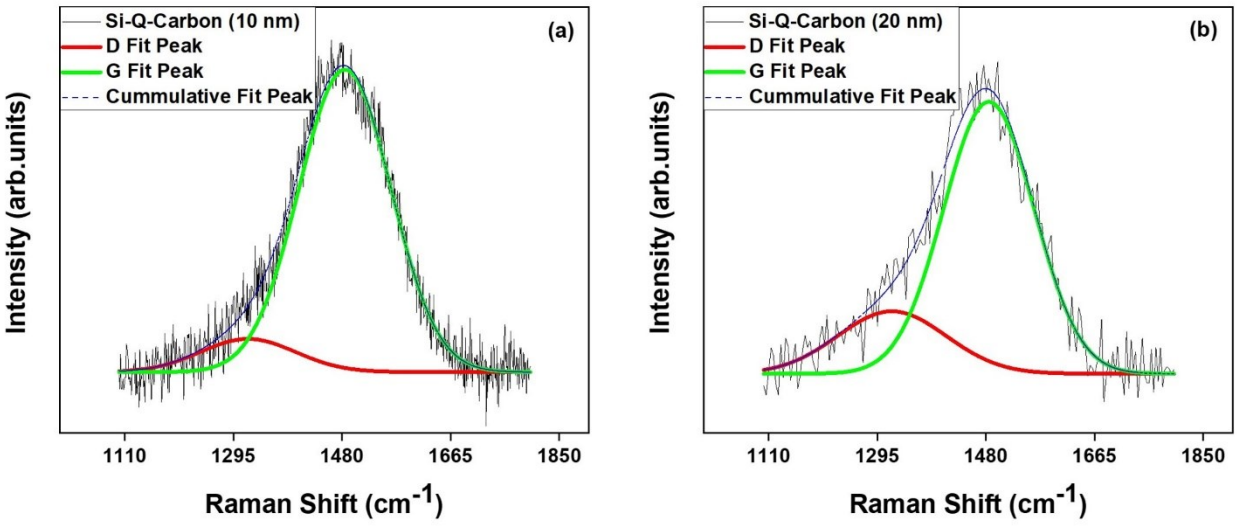

Figure 3. *The Raman spectra of Si-Q-Carbon samples with a thickness of: (a) 10 nm, (b) 20 nm.*

The XPS measurements were performed to determine the surface composition and understand the bonding characteristics of the samples. Figure 4 shows the XPS survey spectra and the % atomic composition of elements present in the Si-Q-carbon samples. Both samples (10 nm and 20 nm) showed the presence of silicon, carbon, and oxygen in their structure. The high-resolution C1s spectra of the samples (Figure 5) indicate the broadening of the C1s band as the sample thickness decreases. This result shows that there is a decrease in the sp^3 content of the samples as the thickness of the sample increases. The deconvoluted bands observed at 283.5, 284, 284.9, 286.4, and 288 eV were ascribed to Si-C bonds, sp^2-hybridized carbon bonds, sp^3-hybridized carbon bonds, C-O bonds, and C=O bonds, respectively [27]. The sp^3 content

of the 10 nm sample is found to be about 85%; this result is higher than previous XPS sp^3 content results for the Si-DLC structures [39]. Thus, XPS results are in excellent agreement with the Raman spectroscopy results.

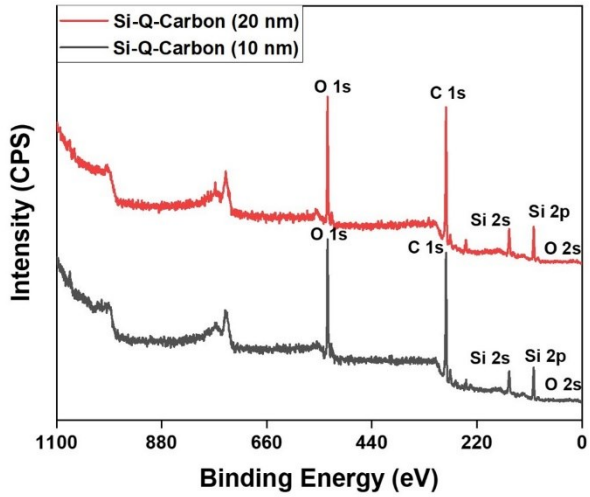

Si-Q-Carbon samples	Elemental atomic % in XP Spectra		
	C 1s	Si 2p	O 1s
10 nm	61.5	19.2	17.5
20 nm	61.8	19.6	16.6

Figure 4. *(a) The XPS spectra of the Si-Q-carbon samples, (b) atomic % of elements present on the surface of the samples.*

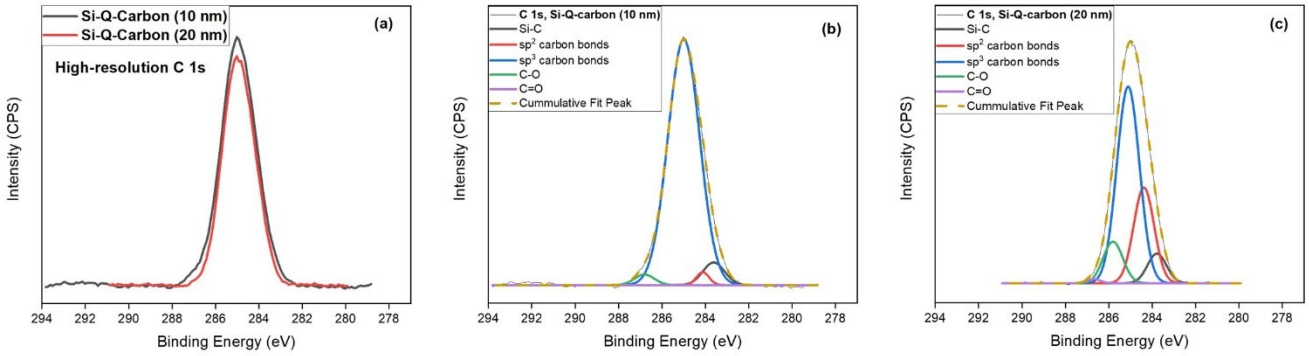

Figure 5. *(a) High-resolution C 1s bands of Si-Q-carbon samples; deconvolution of the C 1s band of Si-Q-carbon samples with a thickness of: (b) 10 nm (c) 20 nm.*

Figure 6 shows the high-resolution transmission electron microscopy (HRTEM) images as well as the corresponding EDS mapping of the elements present in the Si-Q-carbon samples. Samples were prepared by focused ion beam (FIB) milling for TEM analysis. The red rectangles in Figures 6(a) and 6(b) show the position of Si-Q-carbon in 10 nm and 20 nm samples, respectively. EDS mapping of elements (Figure 6(c) and 6(d)) shows the presence of carbon, oxygen, and silicon as indicated in green, red, and orange colors, respectively. Green color dominates both the samples, indicating the presence

of carbon as the main element in the sample. The SiO_x layer in the substrate is observed below the Si-Q-carbon layer in the samples.

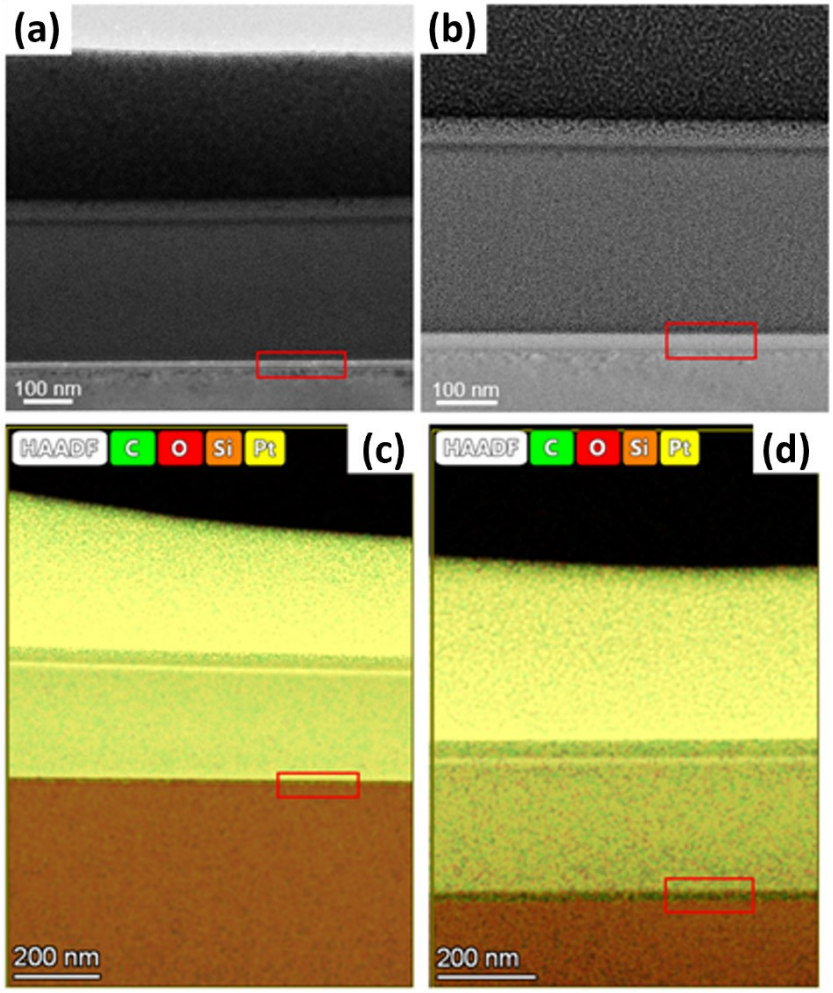

Figure 6. *The high-resolution TEM images of Si-Q-carbon with a thickness of: (a) 10 nm (b) 20 nm. Corresponding EDS maps of Si-Q-carbon samples with a thickness of: (c) 10 nm (d) 20 nm.*

Room-temperature electron energy-loss spectroscopy (EELS) was carried out to validate the sp^3 content present in the films. It is shown that a typical EEL spectrum of Q-carbon consists of π^* and σ^* bands, corresponding to sp^2 and sp^3 hybridized orbitals in the material, respectively [42]. As such, the Gaussian fitting of the C-K edges of Si-Q-Carbon samples shows three characteristic peaks associated with C=C π^*, C=C σ_1^*, and C-C σ_2^* as shown in Figure 7. Cuomo et al. have shown that the sp^2 content in a carbon film can be determined from EEL spectrum using the following equation [41].

$$\frac{(\pi^*/\sigma^*)_{\text{carbon structure}}}{(\pi^*/\sigma^*)_{\text{standard}}} = \frac{3x}{4-x} \qquad (7)$$

In this equation, x is the sp^2 fraction, and $(\pi^*/\sigma^*)_{standard}$ is the π^*/σ^* value for graphite, which is equal to 0.33. Graphite is considered as a standard reference as it is composed of 100% sp^2-hybridized bonds [41-42]. Solving the equation yields a sp^2 fraction of ~14% and ~23% in 10-nm and 20-nm samples, respectively; the highest percentage of sp^3 content (~86%) was noted in the thinnest sample. These results are consistent with the data obtained from XPS and Raman spectroscopy.

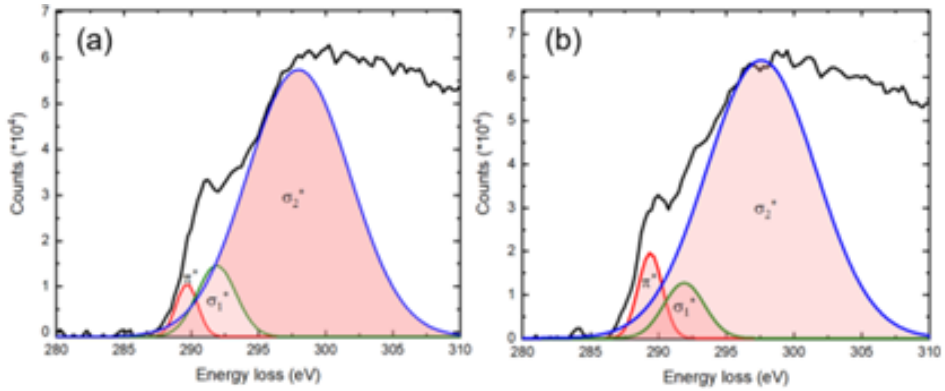

Figure 7. *Fitted EEL spectra (C-K edges) of Si-Q-carbon samples with a thickness of (a) 10 nm (b) 20 nm.*

The water contact angle optical images are shown in Figure 8; measurements of 75.3° (± 0.6°) and 78.8° (± 0.1°) were obtained for 10 nm and 20 nm thick samples, respectively. Figure 9 shows the dispersive and polar components of surface energies of the films as assessed using Equation 2(a). It is known that the polar component of the surface energy leads to the hydrophobic character in the film. While the total surface free energy of the thin films increases from 22.7 mN/m to 30.5 mN/m, the subsequent polar component decreases from 8.6 mN/m to 8.0 mN/m as the film thickness was reduced from 20 nm to 10 nm. This result confirms the hydrophilic character in the 10 nm Si-Q-carbon thin film. Previous reports on the surface energy properties of Si-DLC thin films have stressed the role of surface plasma treatment to improve the wettability of films [43]. In this study, we demonstrate that the as-deposited Si-Q-carbon films are hydrophilic without post-processing treatments. Furthermore, Roy et al. have shown that surface wettability is closely related to the polar component of surface energy, which in turn is determined by the polarizability of the surface chemical bonds [50]. Thus, the 10 nm Si-Q-carbon sample with high surface energy and the larger sp^3/sp^2 value shows enhanced wettability as compared to the 20 nm thick sample.

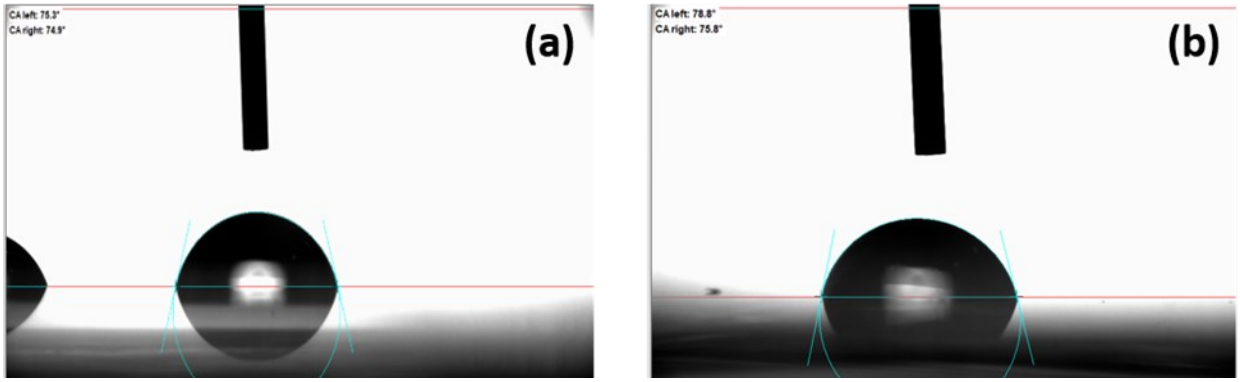

Figure 8. *Water contact angle for Si-Q-Carbon samples with a thickness of: (a) 10 nm (75.3° (± 0.6°)) and (b) 20 nm. Fiducial marks in the image represent the reference point (0°) of the drop profile.*

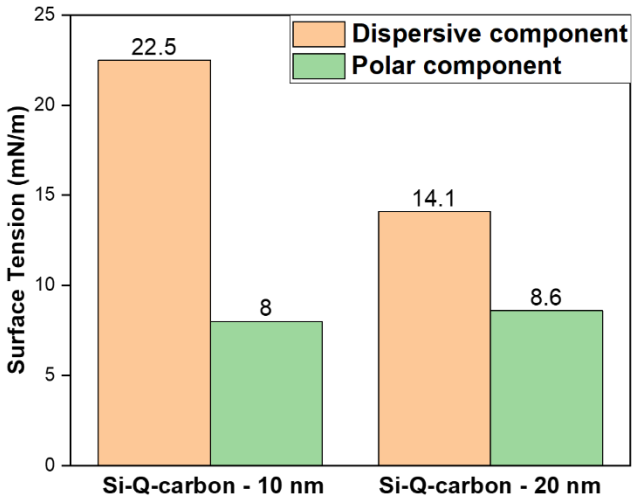

Figure 9*. Polar and dispersive component of surface energies of Si-Q-carbon thin films.*

Figure 10 shows the quantitative assessment of the adhesion of both viable and non-viable bacteria for the Si-Q-carbon thin films with three replicates for each sample evaluated (n = 9 total measurements; 3 per replicate). Figure 11 contains the merged DAPI and Sytox fluorescence images that were acquired from the stained bacteria (*S. epidermidis)* after 24 hours of exposure to the Si-Q-carbon thin films. The green colored stain indicates the dead bacteria, and the blue colored stain indicates the presence of active and living bacteria. Between the two samples, 10 nm thick Si-Q-carbon showed a higher reduction of biofilm adhesion compared to the glass control (57%, DAPI; Fig.10); in contrast, the 20 nm sample was markedly less effective (7%). Furthermore, it is established that the adhesion of bacteria to the surface is dependent on (a) sp^3-bonding and (b) surface hydrophobicity [44-45]. Zhao et al. have shown that bacterial adhesion is significantly

reduced with the increase in the sp^3/sp^2 value in DLC thin films [52]. As such, the repulsion of water by the hydrophobic surface could allow the cells to lie closer to the liquid-solid interface, which could allow the attachment of bacterial cells to the surface [45-49]. Consequently, the sample with the highest sp^3 content and hydrophilic surface showed enhanced resistance to bacterial growth and thus possessed superior antimicrobial properties.

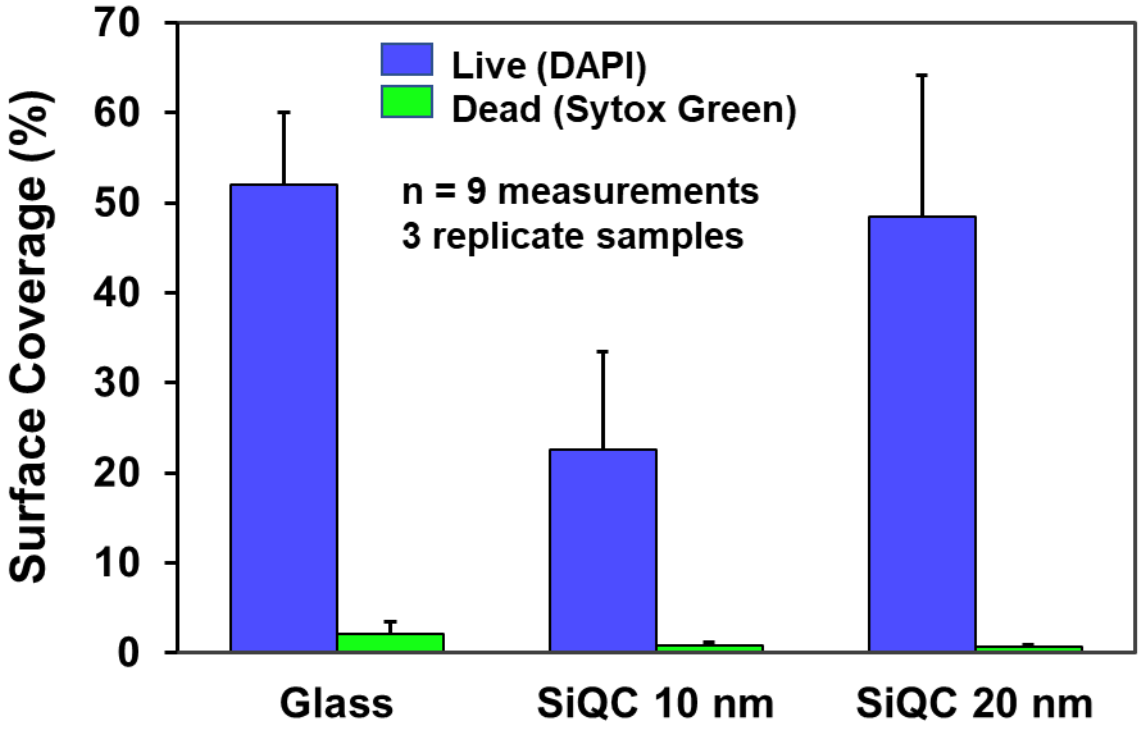

Figure 10. *Quantification of bacteria surface coverage on Si-Q-carbon thin films.*

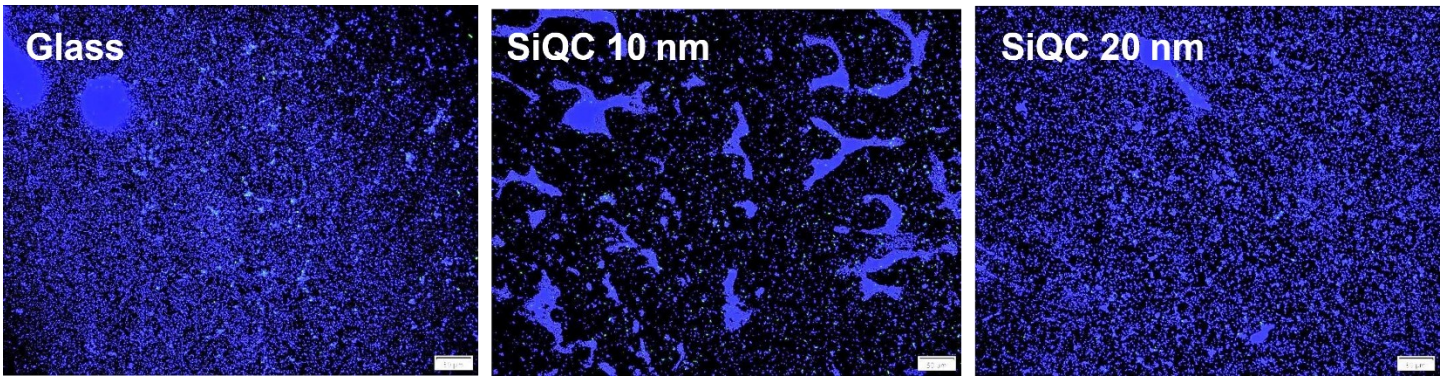

Figure 11. *Merged DAPI (blue) and Sytox (green) fluorescence images of S. epidermidis. Scale bar length = 50 µm.***4.**

Conclusions

In this study, Si-incorporated Q-carbon coatings with different thickness values (10 nm, 20 nm) were deposited through the PECVD technique. Raman spectroscopy, XPS, and EELS studies were performed to assess the surface composition and

quantify the sp^3/sp^2 value in the thin films. Water contact angle assessments and surface energy calculations were undertaken to evaluate the hydrophilicity of the films. The interaction of *S. epidermidis* with the 10 nm and 20 nm Si-Q-carbon samples was studied by fluorescence microscopy and biofilm adhesion; activity was quantified by the percent area coverage of live and dead bacteria. The film with a thickness of 10 nm was found to be hydrophilic, with higher sp^3 bonding (85%) characteristics; it showed a substantial reduction in biofilm adhesion (57%) as compared to the thicker film sample (7%). The enhanced antibacterial activity of Q-carbon thin film is attributed to its hydrophilicity and tunable surface characteristics. Since a large number of medical implant-related infections are associated with complex interactions among the pathogen, the host, and the implant, the development of multifunctional antibacterial surface treatments to prevent implant infections can be of significant importance [53]. In addition to enhanced antibacterial characteristics, the Q-carbon has higher hardness, toughness, and adhesion, making Q-carbon coatings more effective in reducing medical implant-related infections.

5. Author Contributions

Naveen Joshi: formal analysis, writing – original draft, conducted the material synthesis, Raman Spectroscopy, XPS, TEM and AFM measurements; Shubhangi Shukla: contact angle measurements; Nayna Khosla: AFM measurements; Lyndsi Vanderwal: antibacterial testing and analysis; Shane Stafslien: antibacterial testing and analysis; Roger Narayan: supervision, conceived the project, and funding; Jagdish Narayan: supervision, conceived the project, and funding.

6. Conflicts of Interest

The authors declare that they have no known financial interests or personal relationships that could have appeared to influence the work reported in this paper.

7. Acknowledgements

The authors would like to thank Bill Kiether for his assistance with the PECVD deposition of Si-Q-Carbon samples. This work was performed in part at the NCSU Nanofabrication Facility (NNF), a member of the North Carolina Research Triangle Nanotechnology Network (RTNN), which is supported by the National Science Foundation (Grant ECCS-1542015) as a part of the Nanotechnology Coordinated Infrastructure (NNCI). The authors would also like to acknowledge the services provided by the Analytical Instrumentation Facility (AIF) at North Carolina State University, which is supported by the state of North Carolina and the National Science Foundation (award number ECCS-2025064). The AIF is a member of the North

Carolina Research Triangle Nanotechnology Network (RTNN), a site in the National Nanotechnology Coordinated Infrastructure (NNCI). Antibacterial testing performed at NDSU was supported by the Office of Naval Research (award number: N00014-20-1-2236). The authors also wish to acknowledge National Science Foundation grants 1836767, 2029974, and 2037636.

8. References

[1] Al-Jumaili, A., Alancherry, S., Bazaka, K. and Jacob, M.V., 2017. Review on the antimicrobial properties of carbon nanostructures. *Materials*, *10*(9), p.1066.

[2] Dearnaley, G. and Arps, J.H., 2005. Biomedical applications of diamond-like carbon (DLC) coatings: A review. *Surface and Coatings Technology*, *200*(7), pp.2518-2524.

[3] Alanazi, A., Nojiri, C., Kido, T., Noguchi, J., Ohgoe, Y., Matsuda, T., Hirakuri, K., Funakubo, A., Sakai, K. and Fukui, Y., 2000. Engineering analysis of diamond-like carbon coated polymeric materials for biomedical applications. *Artificial Organs*, *24*(8), pp.624-627.

[4] Tran, H.S., Puc, M.M., Hewitt, C.W., Soll, D.B., Marra, S.W., Simonetti, V.A., Cilley, J.H. and DelRossi, A.J., 1999. Diamond-like carbon coating and plasma or glow discharge treatment of mechanical heart valves. *Journal of Investigative Surgery*, *12*(3), pp.133-140.

[5] Tran, H.S., Puc, M.M., Hewitt, C.W., Soll, D.B., Marra, S.W., Simonetti, V.A., Cilley, J.H. and DelRossi, A.J., 1999. Diamond-like carbon coating and plasma or glow discharge treatment of mechanical heart valves. *Journal of Investigative Surgery*, *12*(3), pp.133-140.

[6] An, X., Wu, Z., Liu, L., Shao, T., Xiao, S., Cui, S., Lin, H., Fu, R.K., Tian, X., Chu, P.K. and Pan, F., 2019. High-ion-energy and low-temperature deposition of diamond-like carbon (DLC) coatings with pulsed kV bias. *Surface and Coatings Technology*, *365*, pp.152-157.

[7] Hainsworth, S.V. and Uhure, N.J., 2007. Diamond like carbon coatings for tribology: production techniques, characterisation methods and applications. *International materials reviews*, *52*(3), pp.153-174.

[8] Voevodin, A.A., Donley, M.S. and Zabinski, J.S., 1997. Pulsed laser deposition of diamond-like carbon wear protective coatings: a review. *Surface and Coatings Technology*, *92*(1-2), pp.42-49.

[9] Anders, S., Anders, A., Brown, I.G., Wei, B., Komvopoulos, K., Ager Iii, J.W. and Yu, K.M., 1994. Effect of vacuum arc deposition parameters on the properties of amorphous carbon thin films. *Surface and coatings technology*, *68*, pp.388-393.

[10] Bociaga, D., Kaminska, M., Sobczyk-Guzenda, A., Jastrzebski, K., Swiatek, L. and Olejnik, A., 2016. Surface properties and biological behaviour of Si-DLC coatings fabricated by a multi-target DC–RF magnetron sputtering method for medical applications. *Diamond and Related Materials*, *67*, pp.41-50.

[11] Abelson, J.R. and Girolami, G.S., 2020. New strategies for conformal, superconformal, and ultrasmooth films by low temperature chemical vapor deposition. *Journal of Vacuum Science & Technology A*, *38*(3).

[12] Ham, M. and Lou, K.A., 1990. Diamond-like carbon films grown by a large-scale direct current plasma chemical vapor deposition reactor: System design, film characteristics, and applications. *Journal of Vacuum Science & Technology A: Vacuum, Surfaces, and Films*, *8*(3), pp.2143-2149.

[13] Zia, A.W. and Birkett, M., 2021. Deposition of diamond-like carbon coatings: Conventional to non-conventional approaches for emerging markets. *Ceramics International*, *47*(20), pp.28075-28085.

[14] Clay, K.J., Speakman, S.P., Morrison, N.A., Tomozeiu, N., Milne, W.I. and Kapoor, A., 1998. Material properties and tribological performance of rf-PECVD deposited DLC coatings. *Diamond and related materials*, *7*(8), pp.1100-1107.

[15] Gotzmann, G., Beckmann, J., Wetzel, C., Scholz, B., Herrmann, U. and Neunzehn, J., 2017. Electron-beam modification of DLC coatings for biomedical applications. *Surface and Coatings Technology*, *311*, pp.248-256.

[16] Wu, W.J. and Hon, M.H., 1999. Thermal stability of diamond-like carbon films with added silicon. *Surface and Coatings Technology*, *111*(2-3), pp.134-140.

[17] Ban, M. and Hasegawa, T., 2003. Internal stress reduction by incorporation of silicon in diamond-like carbon films. *Surface and Coatings Technology*, *162*(1), pp.1-5.

[18] Liu, C., Zhao, Q., Liu, Y., Wang, S. and Abel, E.W., 2008. Reduction of bacterial adhesion on modified DLC coatings. *Colloids and Surfaces B: Biointerfaces*, *61*(2), pp.182-187.

[19] Zhao, J.F., Lemoine, P., Liu, Z.H., Quinn, J.P. and McLaughlin, J.A., 2000. The effects of Si incorporation on the microstructure and nanomechanical properties of DLC thin films. *Journal of Physics: Condensed Matter*, *12*(44), p.9201.

[20] Rao, X., Yang, J., Chen, Z., Yuan, Y., Chen, Q., Feng, X., Qin, L. and Zhang, Y., 2020. Tuning C–C sp2/sp3 ratio of DLC films in FCVA system for biomedical application. *Bioactive Materials*, *5*(2), pp.192-200.

[21] Yang, K. H., Riley, P., Rodenhausen, K. B., Skoog, S. A., Stafslien, S. J., Vanderwal, L., & Narayan, R. J., 2022. Antifungal behavior of silicon-incorporated diamond-like carbon by tuning surface hydrophobicity with plasma treatment. *International Journal of Applied Ceramic Technology*.

[22] Yu, Y., Tang, W., Liu, Z. and Bai, L., 2020. Deformation mechanisms of Si-doped diamond-like carbon films under uniaxial tension conditions. *Diamond and Related Materials*, *110*, p.108099.

[23] Reisel, G., Steinhäuser, S. and Wielage, B., 2004. The behaviour of DLC under high mechanical and thermal load. *Diamond and related materials*, *13*(4-8), pp.1516-1520.

[24] Narayan, J. and Bhaumik, A., 2015. Novel phase of carbon, ferromagnetism, and conversion into diamond. *Journal of Applied Physics*, *118*(21), p.215303.

[25] Bhaumik, A. and Narayan, J., 2018. Electrochromic effect in Q-carbon. *Applied Physics Letters*, *112*(22), p.223104.

[26] Joshi, P., Gupta, S., Haque, A. and Narayan, J., 2020. Fabrication of ultrahard Q-carbon nanocoatings on AISI 304 and 316 stainless steels and subsequent formation of high-quality diamond films. *Diamond and Related Materials*, *104*, p.107742.

[27] Riley, P.R., Joshi, P., Khosla, N., Narayan, R.J. and Narayan, J., 2022. Formation of Q-carbon with wafer scale integration. *Carbon*, *196*, pp.972-978.

[28] Vuong, C. and Otto, M., 2002. Staphylococcus epidermidis infections. *Microbes and infection*, *4*(4), pp.481-489.

[29] França, Â.M.O.S., Freitas, A.I.C., Carvalhais, V.M.D., Pérez-Cabezas, B., Correia, A., Cywes-Bentley, C., Maira-Litrán, T., Vilanova, M., Pier, G.B. and Cerca, N., 2013. Staphylococcus epidermidis biofilm lifecycle and its virulence: from plantkonic growth, to biofilm structure and systemic dissemination.

[30] Khosla N. Laser Processing of Q-Carbon, Diamond, and Anode and Cathode for Lithium-Ion Batteries. North Carolina State University; 2023.

[31] Owens, D.K. and Wendt, R.C., 1969. Estimation of the surface free energy of polymers. *Journal of applied polymer science*, *13*(8), pp.1741-1747.

[32] Fowkes, F.M., 1963. Additivity of intermolecular forces at interfaces. i. determination of the contribution to surface and interfacial tensions of dispersion forces in various liquids1. *The Journal of Physical Chemistry*, *67*(12), pp.2538-2541.

[33] Van Oss, C.J., Chaudhury, M.K. and Good, R.J., 1988. Interfacial Lifshitz-van der Waals and polar interactions in macroscopic systems. *Chemical reviews*, *88*(6), pp.927-941.

[34] Pezzotti, G., Bock, R.M., McEntire, B.J., Adachi, T., Marin, E., Boschetto, F., Zhu, W., Mazda, O. and Bal, S.B., 2018. In vitro antibacterial activity of oxide and non-oxide bioceramics for arthroplastic devices: I. In situ time-lapse Raman spectroscopy. *Analyst*, *143*(15), pp.3708-3721.

[35] Al-Amshawee, S., Yunus, M.Y.B.M., Lynam, J.G., Lee, W.H., Dai, F. and Dakhil, I.H., 2021. Roughness and wettability of biofilm carriers: A systematic review. *Environmental Technology & Innovation*, *21*, p.101233.

[36] Ahmad, M., Liu, S., Mahmood, N., Mahmood, A., Ali, M., Zheng, M. and Ni, J., 2017. Effects of porous carrier size on biofilm development, microbial distribution and nitrogen removal in microaerobic bioreactors. *Bioresource technology*, *234*, pp.360-369.

[37] Ahmed, M.H., Byrne, J.A. and Ahmed, W., 2015. Characteristic of silicon doped diamond like carbon thin films on surface properties and human serum albumin adsorption. *Diamond and Related Materials*, *55*, pp.108-116.

[38] Dychalska, A., Popielarski, P., Franków, W., Fabisiak, K., Paprocki, K. and Szybowicz, M., 2015. Study of CVD diamond layers with amorphous carbon admixture by Raman scattering spectroscopy. *Mater. Sci.-Pol*, *33*(4), pp.799-805.

[39] Riley, P.R., Joshi, P., Penchev, H., Narayan, J. and Narayan, R.J., 2021. One-Step Formation of Reduced Graphene Oxide from Insulating Polymers Induced by Laser Writing Method. *Crystals*, *11*(11), p.1308.

[40] Riley, P.R., Joshi, P., Azizi Machekposhti, S., Sachan, R., Narayan, J. and Narayan, R.J., 2021. Enhanced Vapor Transmission Barrier Properties via Silicon-Incorporated Diamond-Like Carbon Coating. *Polymers*, *13*(20), p.3543.

[41] Cuomo, J.J., Doyle, J.P., Bruley, J. and Liu, J.C., 1991. Sputter deposition of dense diamond-like carbon films at low temperature. *Applied physics letters*, *58*(5), pp.466-468.

[42] Daniels, H., Brydson, R., Rand, B. and Brown, A., 2007. Investigating carbonization and graphitization using electron energy loss spectroscopy (EELS) in the transmission electron microscope (TEM). *Philosophical Magazine*, *87*(27), pp.4073-4092.

[43] Movahed, S., Nguyen, A.K., Goering, P.L., Skoog, S.A. and Narayan, R.J., 2020. Argon and oxygen plasma treatment increases hydrophilicity and reduces adhesion of silicon-incorporated diamond-like coatings. *Biointerphases*, *15*(4), p.041007.

[44] Roy, R.K., Choi, H.W., Park, S.J. and Lee, K.R., 2007. Surface energy of the plasma treated Si incorporated diamond-like carbon films. *Diamond and Related Materials*, *16*(9), pp.1732-1738.

[45] R. Oliveira, J. Azeredo, P. TeixeiraA. P. Fonseca. The role of hydrophobicity in bacterial adhesion, in: P Guilbert Ed., Biofilm Community Interactions, Chance Or Necessity? Contributions Made at the Fifth Meeting of the Biofilm Club Held at Gregynog Hall, Powys, U.K. 13-15 September, 2001, Bioline, 2002, pp. 11-22. https://hdl.handle.net/1822/6706

[46] Zhao, Q., Liu, Y., Wang, C. and Wang, S., 2007. Evaluation of bacterial adhesion on Si-doped diamond-like carbon films. *Applied Surface Science*, *253*(17), pp.7254-7259.

[47] Yang, L., Wang, C., Li, L., Zhu, F., Ren, X., Huang, Q., Cheng, Y. and Li, Y., 2022. Bioinspired integration of naturally occurring molecules towards universal and smart antibacterial coatings. *Advanced Functional Materials*, *32*(4), p.2108749.

[48] Joshi, P., Shukla, S., Gupta, S., Joshi, N., Narayan, J. and Narayan, R., 2023. Synthesis of laser-patterned MoS2 nanoneedles for advanced electrochemical sensing. *MRS Communications*, pp.1-7.

[49] Pandey, P.C., Shukla, S., Pandey, G. and Narayan, R.J., 2020. Organotrialkoxysilane-mediated synthesis of functional noble metal nanoparticles and their bimetallic for electrochemical recognition of L-tryptophan. *MRS Advances*, *5*(46-47), pp.2429-2444.